ORIGINAL ARTICLE

Effects of mTOR inhibition on cardiac and adipose tissue pathology and glucose metabolism in rats with metabolic syndrome

Ayako Uchinaka[1], Mamoru Yoneda[1], Yuichiro Yamada[1], Toyoaki Murohara[2] & Kohzo Nagata[1] (iD)

[1]Department of Pathophysiological Laboratory Sciences, Nagoya University Graduate School of Medicine, Nagoya, Japan
[2]Department of Cardiology, Nagoya University Graduate School of Medicine, Nagoya, Japan

Abstract

The mammalian target of rapamycin (mTOR) is a regulator of metabolism and is implicated in pathological conditions such as obesity and diabetes. We aimed to investigate the role of mTOR in obesity. A new animal model of metabolic syndrome (MetS), named DahlS.Z-$Lepr^{fa}$/$Lepr^{fa}$ (DS/obese) rats was established previously in our laboratory. In this study, we used this model to evaluate the effects of mTOR inhibition on cardiac and adipose tissue pathology and glucose metabolism. DS/obese rats were treated with the mTOR inhibitor, everolimus, (0.83 mg/kg per day, per os) for 4 weeks at 9 weeks of age. Age-matched homozygous lean (DahlS.Z-$Lepr^+$/$Lepr^+$ or DS/lean) littermates of DS/obese rats were used as controls. Treatment with everolimus ameliorated hypertension, left ventricular (LV) hypertrophy and fibrosis, and LV diastolic dysfunction, and attenuated cardiac oxidative stress and inflammation in DS/obese rats, but had no effect on these parameters in DS/lean rats. Treatment with everolimus reduced Akt Thr308 phosphorylation in the heart of DS/obese rats. It also alleviated obesity, hyperphagia, adipocyte hypertrophy, and adipose tissue inflammation in DS/obese rats. Everolimus treatment exacerbated glucose intolerance, but did not affect Akt phosphorylation levels in the fat or liver in these rats. Pancreatic β-cell mass was increased in DS/obese rats compared with that in DS/lean rats and this effect was attenuated by everolimus. Activation of mTOR signaling contributes to the pathophysiology of MetS and its associated complications. And mTOR inhibition with everolimus ameliorated obesity as well as cardiac and adipose tissue pathology, but exacerbated glucose metabolism in rats with MetS.

Abbreviations

11β-HSD1, 11β-1hydroxysteroid dehydrogenase type 1; ALT, alanine aminotransferase; AMPK, AMP-activated protein kinase; ANP, atrial natriuretic peptide; AST, aspartate aminotransferase; BNP, brain natriuretic peptide; BUN, blood urea nitrogen; COX-2, cyclooxygenase-2; DAB, 3,3'-diaminobenzidine; DcT, deceleration time; DS/lean, DahlS.Z-$Lepr^+$/$Lepr^+$; DS/obese, DahlS.Z-$Lepr^{fa}$/$Lepr^{fa}$; E/A, the ratio of peak flow velocity at the mitral level during rapid filling (E) to that during atrial contraction (A); Eve, everolimus; FKBP12, FK506-binding protein12; G6Pase, glucose 6-phosphatase; GAPDH, glyceraldehyde-3-phosphate dehydrogenase; GR, glucocorticoid receptor; GSI, glomerulosclerosis index; HDL-cholesterol, high-density lipoprotein-cholesterol; HOMA, homeostasis model assessment; HOMA-IR, HOMA of insulin resistance; HOMA-β, HOMA for β-cell function; IRT, isovolumic relaxation time; ITT, insulin tolerance test; IVST, interventricular septum thickness;

LDL-cholesterol, low-density lipoprotein-cholesterol; LVDd, LV end-diastolic dimension; LVDs, LV end-systolic dimension; LVEDP, LV end-diastolic pressure; LVEF, LV ejection fraction; LVFS, LV fractional shortening; LV, left ventricular; LVPWT, LV posterior wall thickness; MCP-1, monocyte chemoattractant protein-1; MetS, metabolic syndrome; mTOR, mammalian target of rapamycin; NADPH, nicotinamide adenine dinucleotide phosphate; OGTT, oral glucose tolerance test; PEPCK, phosphoenolpyruvate carboxykinase; PI3K, phosphoinositide 3-kinase; RT-PCR, reverse-transcription polymerase chain reaction; RWT, relative wall thickness; SBP, systolic blood pressure; SREBP-1c, sterol regulatory element-binding protein 1c; TGF-β1, transforming growth factor-β1; TIS, tubulointerstitial injury score.

Introduction

The mammalian target of rapamycin (mTOR) is a serine/threonine kinase and is a component of a complex signaling pathway involved in energy and nutrient abundance, and metabolism (Yuan et al. 2009). The mTOR signaling pathway is implicated in a number of pathological conditions, including obesity and type II diabetes (Laplante and Sabatini 2012), and its role in regulating growth and metabolism has garnered attention in the last few years.

mTOR is found in two distinct protein complexes: mTOR complex 1 (mTORC1), which regulates pathways involved in mRNA translation, protein synthesis, and cell growth; and mTOR complex 2 (mTORC2), which regulates the cytoskeleton and insulin signaling (Hughes and Kennedy 2012). Rapamycin specifically inhibits mTORC1, but chronic treatment with rapamycin in vitro and in vivo inhibits both mTORC1 and mTORC2 (Sarbassov et al. 2006). Everolimus is an orally available mTOR inhibitor structurally related to rapamycin (Goudar et al. 2005)that interferes with the assembly of both mTORC1 and mTORC2 (Mancini et al. 2010). mTOR inhibitors such as rapamycin or everolimus have an inhibitory effect on protein synthesis through direct repression of mTOR. Because of their immunosuppressant actions, mTOR inhibitors have been mainly used in transplantation medicine. However, they are also used as anti-proliferative agents for coating drug-eluting stents to reduce restenosis after coronary angioplasty (Hausleiter et al. 2004; Stone et al. 2016). In the context of cardiac hypertrophy, recent studies indicate that rapamycin and everolimus haves inhibitory effects on the development of load-induced left ventricular (LV) hypertrophy (Shioi et al. 2003) and of LV remodeling after myocardial infarction (Buss et al. 2009), respectively. However, the effects of mTOR inhibition on cardiac and adipose tissue pathology and on glucose and lipid metabolism in metabolic disorders remain elusive.

Our laboratory recently characterized a novel animal model for metabolic syndrome (MetS), the DahlS.Z-*Lepr*^fa^/*Lepr*^fa^ (DS/obese) rat, by crossing Dahl salt-sensitive (DS) rats with Zucker rats carrying a missense mutation in the leptin receptor gene (*Lepr*) (Hattori et al.

2011). When fed a normal diet, DS/obese rats develop a phenotype similar to human MetS, including hypertension. They also develop cardiac injury and fat-induced liver damage (Hattori et al. 2011) as well as LV diastolic dysfunction and LV hypertrophy and fibrosis, which are associated with increased cardiac oxidative stress and inflammation (Murase et al.2012a). To test the role of mTOR in metabolic disorders, we examined the effects of the mTOR inhibitor, everolimus, on cardiac and adipose tissue pathology and glucose and lipid metabolism in DS/obese rats.

Materials and Methods

Animals

All animal experiments were conducted with the approval of the Animal Experiment Committee of Nagoya University Graduate School of Medicine (Daiko district, approval nos. 024-031, 025-013, 026-018, 027-007, and 028-009). Animals were cared for according to the Regulations for Animal Experiments at Nagoya University, following the Guide for the Care and Use of Laboratory Animals [U.S. National Institutes of Health (NIH) publication no. 85-23, revised 2011]. Eight-week-old male inbred DS/obese rats and their lean littermates (DahlS.Z-*Lepr*^+^/*Lepr*^+^, or DS/lean, rats (Cont)) were purchased from Japan SLC Inc. (Hamamatsu, Japan). DS/obese rats were randomly assigned to the mTOR inhibitor everolimus (MetS + Eve, 0.83 mg per kg of body weight per day, LC Laboratories, Woburn, MA) or vehicle (MetS) groups at 9 weeks of age. Everolimus was administered orally once daily via a gastric tube. The dose of everolimus was determined on the basis of results of previous studies and our preliminary observations (Buss et al. 2009).

Glucose tolerance test and insulin tolerance test

The oral glucose tolerance test (OGTT) and the insulin tolerance test (ITT) were performed as previously

described (Takeshita et al. 2015). Tail blood glucose levels were measured using a glucose analyzer (Glutest Neo Super; Sanwa Kagaku Kenkyusho Co. Ltd., Nagoya, Japan).

Cardiac function

Systolic blood pressure (SBP) and heart rate were measured weekly in awake animals by tail-cuff plethysmography (BP-98A; Softron, Tokyo, Japan). Transthoracic echocardiography (Nagata et al. 2002) and cardiac catheterization (Kato et al. 2008) were performed in anesthetized animals at 13 weeks of age, as previously described.

Superoxide production

Nicotinamide adenine dinucleotide phosphate (NADPH)-dependent superoxide production by the LV tissue and the amount of in situ LV myocardium superoxide formation was measured, as described previously (Elmarakby et al. 2005; Nagata et al. 2006).

Biochemical analysis, Histological analysis, Quantitative real-time PCR analysis, and Immunoblot analysis

These assays were performed as described in the supporting information.

Statistical analysis

Data are presented as means ± SEM. Differences among groups of rats at 13 weeks of age were assessed with one-way factorial analysis of variance (ANOVA) and Fisher's multiple comparison test. The time courses of body weight, food intake, water intake, SBP, and heart rate were compared among groups by two-way repeated-measures ANOVA. The independent or interactive influence of rat genotype and everolimus treatment on various parameters in the four experimental groups was evaluated with two-way factorial ANOVA. A $P < 0.05$ was considered statistically significant.

Results

Physiological data and cardiac function

Both body weight and food intake were increased in the MetS group compared with those in the Cont group at 9 weeks of age and thereafter; these effects were markedly attenuated in the MetS + Eve group (Fig. 1A and B). The increase in water intake in the MetS group was further enhanced by everolimus at 10 and 11 weeks (Fig. 1C). However, there was no significant difference at 13 weeks between the MetS and MetS + Eve groups. SBP in the MetS group was also higher than that in the Cont group at 9 weeks of age and thereafter; this increase was substantially attenuated in the MetS + Eve group (Fig. 1D). In contrast, DS/lean rats treated with everolimus exhibited an increase in SBP. The heart rate was lower in the MetS group than in the Cont group and at 9 weeks of age and thereafter; this parameter was reduced by everolimus in both rat strains (Fig. 1E). At 13 weeks of age, the ratios of both the heart and LV weight normalized by tibial length, indices of cardiac and LV hypertrophy, were greater in the MetS group than those in the Cont group, and these effects were attenuated in the MetS + Eve group (Table 1). The ratios of visceral (retroperitoneal and epididymal) and subcutaneous (inguinal) fat weight normalized by tibial length were also increased in the MetS group, and these changes were attenuated by everolimus (Table 1). In contrast, the ratio of liver weight normalized by tibial length was increased and that of pancreas weight was reduced in the MetS group, and these changes were not affected by administration of everolimus.

Echocardiography revealed that interventricular septum (IVST) and LV posterior wall (LVPWT), LV mass, and relative wall thickness (RWT) were significantly increased in the MetS group compared with the Cont group (Table 1). Treatment of DS/obese rats with everolimus attenuated all of these changes. LV fractional shortening (LVFS) and LV ejection fraction (LVEF) were greater in the MetS group than in the Cont group, and everolimus did not affect these parameters. The deceleration time (DcT), isovolumic relaxation time (IRT), and τ were significantly extended, and the E/A was significantly decreased in the MetS group compared to that in the Cont group. The ratio of LV end-diastolic pressure (LVEDP) to LV end-diastolic (LVDd), an index of LV diastolic stiffness, was also increased in the MetS group. These changes in DcT, τ, the E/A, and the LVEDP:LVDd ratio were attenuated in the MetS + Eve group. These data indicate that everolimus attenuated LV diastolic dysfunction in DS/obese rats.

Cardiomyocyte hypertrophy and fibrosis

The cross-sectional area of LV cardiomyocytes was greater in the MetS group than in the Cont group and this increase was attenuated in the MetS + Eve group (Fig. 2A, B). The upregulation of atrial natriuretic peptide (ANP) and brain natriuretic peptide (BNP) genes in the heart of DS/obese rats was attenuated by everolimus (Fig. 2C and D). The extent of fibrosis detected by
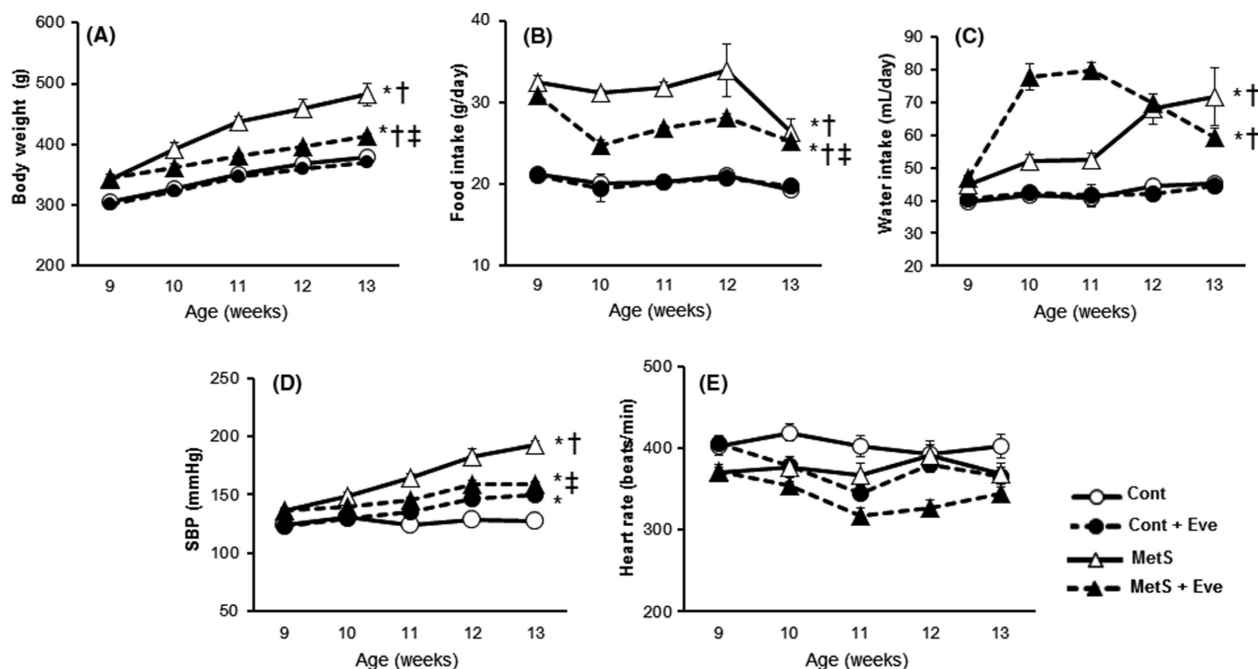
Figure 1. Chronic effects of everolimus on body weight, food intake, systolic blood pressure, and heart rate in DS/obese and control rats from 9 to 13 weeks of age. (A, B) Body weight and food intake were measured weekly. (C, D) Systolic blood pressure and heart rate were measured once every week by the tail-cuff method. Values are presented as means ± SEM for animals. [n = 8, 10, 7, and 12 for Cont, Cont + Eve, MetS, and MetS + Eve]. *$P < 0.05$ versus Cont, †$P < 0.05$ versus Cont+Eve, ‡$P < 0.05$ versus MetS.

Azan-Mallory staining in perivascular and interstitial regions of the LV myocardium was increased in the MetS group compared with the Cont group and this effect was suppressed in the MetS + Eve group (Fig. 2E–H). The levels of collagen type I and III and transforming growth factor (TGF)-β1 mRNAs were increased in the MetS group, and these effects were alleviated in the MetS + Eve group (Fig. 2I–K).

Cardiac inflammation and oxidative stress

Immunostaining of the LV myocardium to identify cells of monocyte/macrophage lineage (CD68) revealed that compared with the Cont group, the MetS group had significantly more monocyte/macrophage in the LV tissue, and administration of everolimus suppressed this increased macrophage infiltration (Fig. 2L and M). The expression of osteopontin, monocyte chemoattractant protein (MCP)-1, and cyclooxygenase (COX)-2 genes in the left ventricle was also upregulated in the MetS group and these effects were prevented in the MetS + Eve group (Fig. 2N–P). Superoxide production in myocardial tissue sections, as revealed by dihydroethidium (DHE)-derived fluorescence imaging, and NADPH oxidase activity in LV homogenates was significantly increased in the MetS group compared to that in the Cont group and these effects were inhibited in the MetS+Eve group (Fig. 3A–C).

Consistent with these effects, the obesity-induced upregulated expression of p22phox and gp91phox mRNAs was also downregulated by everolimus (Fig. 3D and E).

Cardiac mTOR and p70S6K pathway

The amounts of phosphorylated forms of p70S6K were increased in the MetS group compared to those in the Cont group and this effect was suppressed in the MetS + Eve group (Fig. 3F). IRS1/Akt signaling pathway is subject to negative feedback regulation by p70S6K activation. The phosphorylation of Akt Thr308 in the heart was reduced in the MetS group and everolimus restored the phosphorylation to a level similar to that in the Cont group (Fig. 3G). In contrast, the amount of Ser473-phosphorylated Akt in the left ventricle was increased in the MetS group compared with the Cont group and this increase was diminished by everolimus (Fig. 3H).

Adipose tissue pathology

The adipocyte size in the epididymal fat was greater in the MetS group than in the Cont group and this enlargement was attenuated by everolimus treatment (Fig. 4A and B). Immunohistochemistry using the macrophage marker, CD68, revealed a marked increase in macrophage infiltration into the adipose tissue in the MetS group

Table 1. Physiological, morphological, and cardiac functional parameters of DS/lean and DS/obese rats treated or not with everolimus at 13 weeks of age.

Parameter	CONT	Cont + Eve	MetS	MetS + Eve
Heart weight/tibial length (mg/mm)	32.19 ± 0.67	33.78 ± 0.76	42.87 ± 0.60[12]	34.12 ± 0.39[13]
LV weight/tibial length (mg/mm)	24.16 ± 0.65	24.17 ± 0.65	32.43 ± 0.51[12]	24.71 ± 0.40[123]
Liver weight/tibial length (mg/mm)	283.30 ± 9.54	296.35 ± 14.18	612.89 ± 31.39[12]	568.94 ± 19.50[12]
Pancreas weight/tibial length (mg/mm)	42.20 ± 3.86	39.44 ± 1.95	28.68 ± 1.66[12]	29.85 ± 1.97[12]
Kidney weight/tibial length (mg/mm)	3029.67 ± 157.04	2920.40 ± 103.09	3350.88 ± 99.12[12]	2522.00 ± 65.15[123]
Retroperitoneal fat weight/tibial length (mg/mm)	111.71 ± 5.99	113.78 ± 2.71	399.11 ± 19.55[12]	334.74 ± 9.21[123]
Epididymal fat weight/tibial length (mg/mm)	122.27 ± 7.33	129.14 ± 3.46	317.03 ± 12.12[12]	242.55 ± 10.15[123]
Inguinal fat weight/tibial length (mg/mm)	195.63 ± 7.15	196.56 ± 8.21	1105.49 ± 59.28[12]	765.81 ± 23.86[123]
IVSTd (mm)	1.63 ± 0.05	1.76 ± 0.04	2.12 ± 0.10[12]	1.63 ± 0.02[123]
LVDd (mm)	8.09 ± 0.22	7.65 ± 0.12	7.58 ± 0.20	8.05 ± 0.07
LVPWTd (mm)	1.56 ± 0.09	1.70 ± 0.06	2.16 ± 0.09[12]	1.68 ± 0.05[3]
LV mass (mg)	948.71 ± 51.33	962.28 ± 30.76	1286.0 ± 64.26[12]	986.71 ± 25.23
RWT	0.39 ± 0.02	0.45 ± 0.02	0.57 ± 0.04[12]	0.41 ± 0.01[3]
FS (%)	32.62 ± 1.67	35.33 ± 1.87	44.43 ± 1.71[12]	38.55 ± 1.09[12]
EF (%)	69.10 ± 2.22	72.20 ± 2.34	82.46 ± 1.65[12]	76.47 ± 1.20[12]
E/A	1.95 ± 0.09	1.72 ± 0.06	1.54 ± 0.13[1]	1.91 ± 0.07[3]
DcT (ms)	33.89 ± 1.40	38.2 ± 1.45	43.45 ± 1.23[12]	35.82 ± 0.68[3]
IRT (ms)	24.22 ± 2.42	31.43 ± 1.47	38.35 ± 1.84[12]	34.39 ± 1.07[3]
Tau (ms)	27.47 ± 0.82	29.01 ± 2.59	36.72 ± 1.45[12]	28.77 ± 1.73[3]
LVEDP/LVDd (mmHg/mm)	0.56 ± 0.04	0.60 ± 0.05	1.08 ± 0.11[12]	0.65 ± 0.05[3]

Values are expressed as means ± SEM for surviving animals (organ weight and echocardiography; $n = 8, 10, 7$, and 12, cardiac catheterization; $n = 4, 5, 3$, and 9 for DS/lean rats treated with vehicle (Cont), DS/lean rats treated with everolimus (Cont + Eve), DS/obese rats treated with vehicle (MetS), and DS/obese rats treated with everolimus (MetS+Eve), respectively).
[1] $P < 0.05$ versus CONT.
[2] $P < 0.05$ versus Cont + Eve.
[3] $P < 0.05$ versus MetS.

(Fig. 4C and D). Rats in the MetS group exhibited more areas of aggregated CD68-positive cells in the extracellular space among adipocytes, forming a typical crown-like structure, than did the other groups of animals (Fig. 4C). The increase in the extent of macrophage infiltration in adipose tissue of DS/obese rats was attenuated by administration of everolimus. The expression of osteopontin and MCP-1 genes was also upregulated in the MetS group and these effects were attenuated by everolimus (Fig. 4E and F).

With regard to insulin signaling in adipose tissue, everolimus led to a reduction of the increased phosphorylation of p70S6K apparent in the MetS group (Fig. 4G). However, the phosphorylation levels of Akt at both Thr308 and Ser437 was unaffected by everolimus (Fig. 4H and I). The treatment with everolimus induced a decline in AMP-activated protein kinase (AMPK) activity (Fig. 4J).

Liver pathology and function

The state of inflammation, including macrophages (CD68-positive) accumulation, and inflammation marker gene expression, osteopontin and MCP-1, in the liver exhibited a significantly worse state in the MetS group than that in the Cont group, and these changes were significantly attenuated in the MetS + Eve group (Fig. 5A–D). The liver histology assessed by hematoxylin-eosin staining revealed that the refined cell arrangement without inflammatory disorder was observed in the Cont and Cont + Eve group. Lipid accumulation in the liver was manifest in the MetS group by the marked increase in fat deposits within liver cells and swelling of hepatocytes, and these histological signs were also observed in the MetS + Eve group (Fig. 5E). Liver transaminases [aspartate aminotransferase (AST) and alanine aminotransferase (ALT)] are useful biomarkers of liver injury. ALT level was elevated in the MetS group, and the rats in the MetS+Eve group showed higher serum levels of ALT and AST than rats in the MetS group (Table S1).

Hepatic gluconeogenesis, glycolysis, and insulin signaling

Lower mRNA levels of gluconeogenic genes, glucocorticoid receptor (GR) (Fig. 5F), glucose 6-phosphatase (G6Pase), (Fig. 5G), phosphoenolpyruvate carboxykinase (PEPCK) (Fig. 5H), except 11β-1hydroxysteroid dehydrogenase
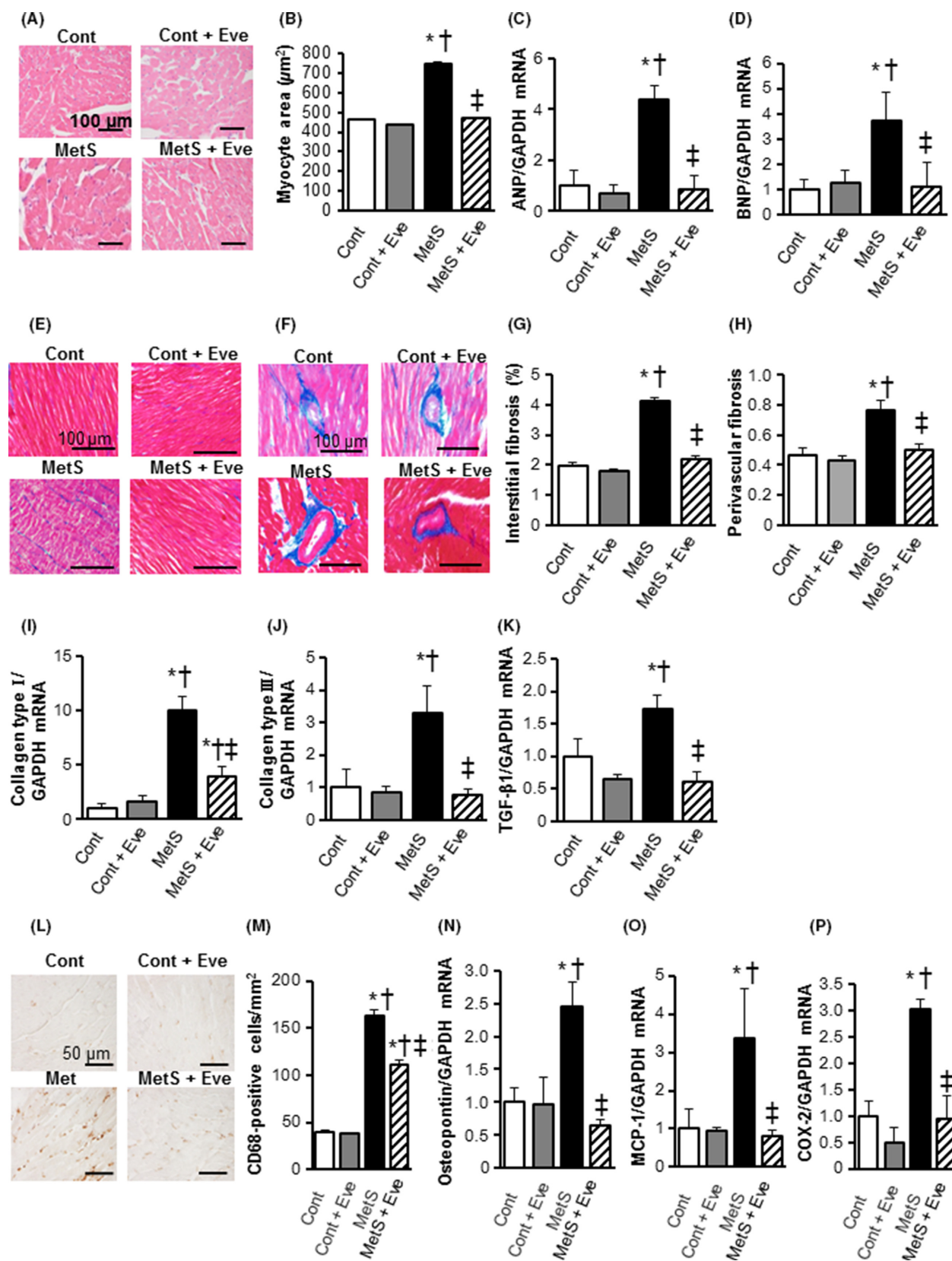
Figure 2. Cardiomyocyte hypertrophy, fibrosis and inflammatory in the left ventricle of rats from the four experimental groups at 13 weeks of age. (A) Representative sections (hematoxylin-eosin stain) of the left ventricular (LV) myocardium. Scale bars show100 μm. (B) Quantitative measurements of cross-sectional area of cardiac myocytes. (C, D) Expression of markers of cardiac hypertrophic response. Atrial natriuretic peptide (ANP, C) and brain natriuretic peptide (BNP, D) mRNA levels measured by RT-PCR in LV tissue samples. Data were normalized to the amount of *Gapdh* mRNA and then expressed relative to the mean value for DS/lean rats treated with vehicle. (E, F) Histological analysis of fibrosis by Azan-Mallory staining in perivascular (upper panels) or interstitial (lower panels) regions in the left ventricular myocardium. Scale bars, 100 μm. (G, H) Percentage of interstitial and perivascular fibrosis in the left ventricular (LV) myocardium. (I–K) Relative mRNA expression of collagen I, III, and transforming growth factor (TGF)-β1 by quantitative PCR. (L) Immunohistochemistry using anti-CD68 in the LV myocardium. Scale bars. 100 μm. (M) Quantification of immunohistochemical CD68 levels. (N–P) mRNA expression levels of the inflammatory markers osteopontin, monocyte chemoattractant protein-1 (MCP-1), and cyclooxygenase (COX)-2 in the left ventricle. Values in (B) through (D), (G) through (K), and (M) through (P) are expressed as means ± SEM for animals. [*n* = 8, 10, 7, and 12 for Cont, Cont + Eve, MetS, and MetS + Eve]. *$P < 0.05$ versus CONT, †$P < 0.05$ versus Cont + Eve, ‡$P < 0.05$ versus MetS.
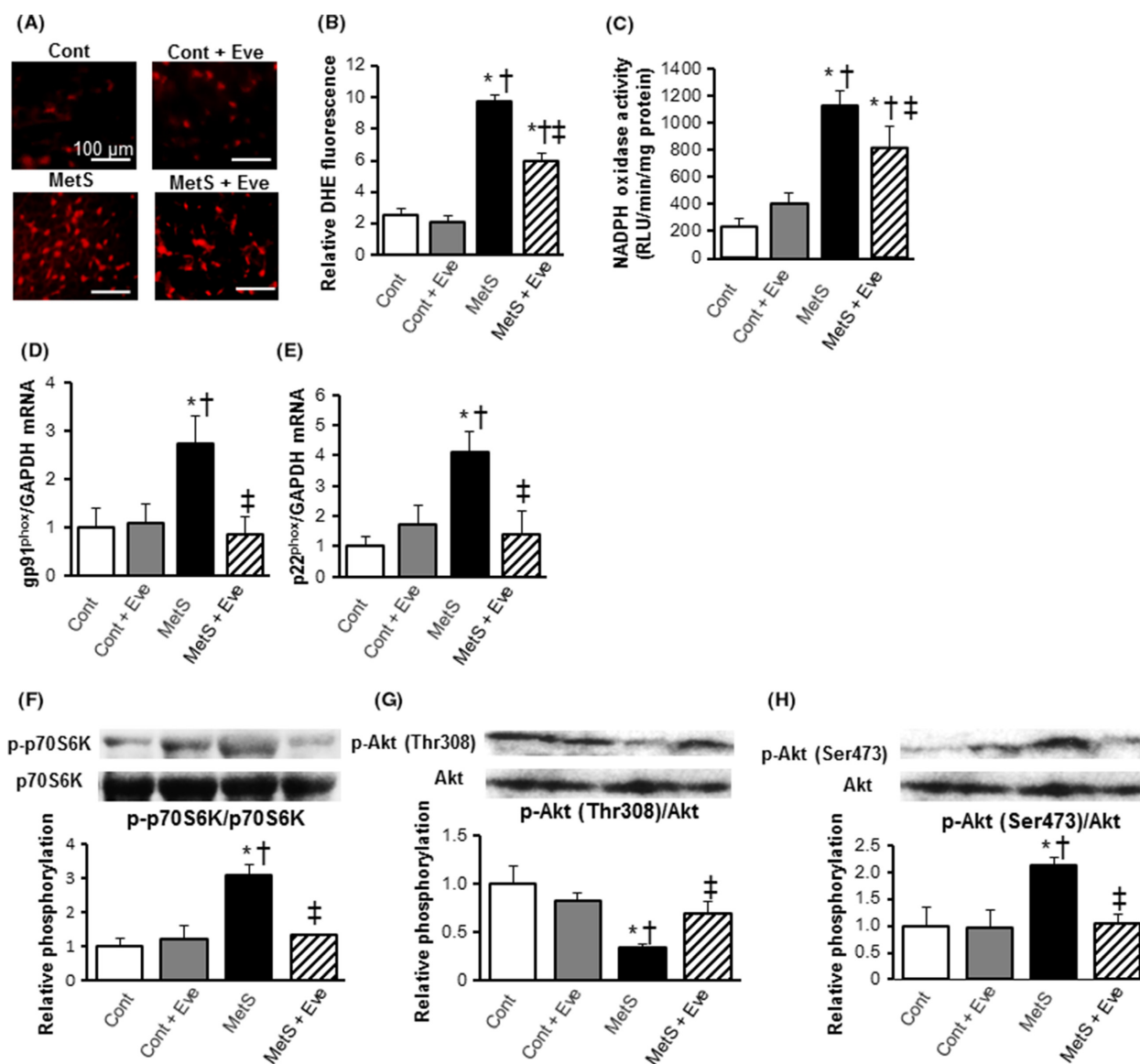

Figure 3. Oxidative stress, and insulin signaling in the left ventricle of rats from the four experimental groups at 13 weeks of age. (A) Impact of everolimus on cardiac oxidative stress level detected by fluorescence dye dihydroethidium (DHE; red spots) Scale bars, 100 μm. (B) DHE-positive area was quantified as a percentage in each total high power field area. (C) Myocardial NADPH oxidase activity (D, E) Quantitative RT-PCR analysis of p22^{phox} and gp91^{phox} mRNAs. (F–H) Evaluation of Akt/mTOR/p70S6K signal activity by western blotting analysis. Levels of phospho-p70S6K (F), phospho-Thr308-Akt (G), and phospho-Ser473-Akt (H). All quantitative data represent means ± SEM. [*n* = 8, 10, 7, and 12 for Cont, Cont + Eve, MetS, and MetS + Eve (A–C) or *n* = 6 for each group (D–H)] *$P < 0.05$ versus CONT, †$P < 0.05$ versus Cont + Eve, ‡$P < 0.05$ versus MetS.
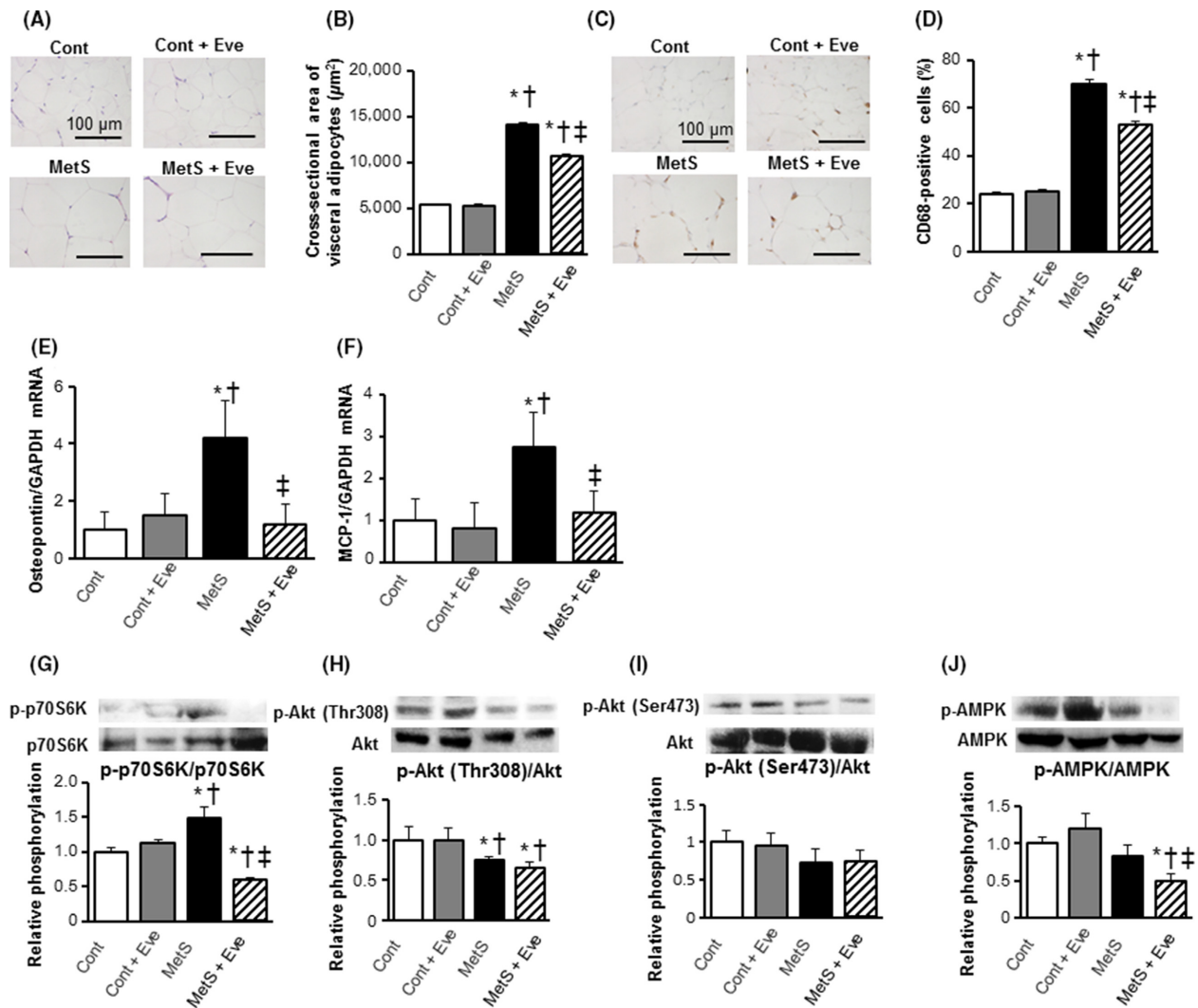
Figure 4. Visceral adipose tissue pathology. (A, B) Histology and mean cross-sectional area of visceral adipocytes. (C) Representative photomicrographs showing immunohistochemical analysis using an anti-CD68 antibody in visceral adipose tissue. Scale bars, 100 μm. (D) Quantification of anti-CD68 positive macrophages as shown in (C). (E, F) mRNA expression levels of the inflammatory markers, osteopontin and monocyte chemoattractant protein-1 (MCP-1). (G–J) Evaluation of insulin signal Akt/mTOR/p70S6K and AMPK activity. Western blot analysis of the phosphorylation of p70S6K (G), Thr308-Akt (H), Ser473-Akt (I), and AMPK (J). All quantitative data represent means $\pm$ SEM. [$n = 8$, 10, 7, and 12 for Cont, Cont+Eve, MetS, and MetS+Eve (B and D–F) or $n = 6$ for each group (G–J)] *$P < 0.05$ versus CONT, †$P < 0.05$ versus Cont + Eve, ‡$P < 0.05$ versus MetS.

Figure 5. Hepatic inflammation, glycometabolism-related gene expression, and insulin signal activity in rats from the four experimental groups at 13 weeks of age. (A) Representative pictures of CD68 -stained liver sections. Scale bars, 100 μm. (B) Morphometrical analysis of CD68 positive cells from (A). (C, D) Gene expression of osteopontin and monocyte chemoattractant protein-1 (MCP-1) in the liver. (E) Representative pictures of hematoxylin and eosin-stained liver tissue sections. (F–I) mRNA levels of gluconeogenic factors, GR, G6Pase, PEPCK, and11β-HSD1, in the liver. (J) mRNA expression levels of the glycolytic factor GK in the liver. (K) mRNA expression levels of the lipogenesis-related factor, SREBP-1c, in the liver. Results in (F–K) are normalized to the levels observed in Cont rats. (L–N) Evaluation of insulin signal Akt/mTOR/p70S6K activity. Western blot analysis of the phosphorylation of p70S6K (L), Thr308-Akt (M), and Ser473-Akt (N). Values in (B) through (J), and (L) through (N) are expressed as means $\pm$ SEM for animals. ($n = 8$, 10, 7, and 12 for Cont, Cont + Eve, MetS, and MetS + Eve) *$P < 0.05$ versus CONT, †$P < 0.05$ versus Cont + Eve, ‡$P < 0.05$ versus MetS.
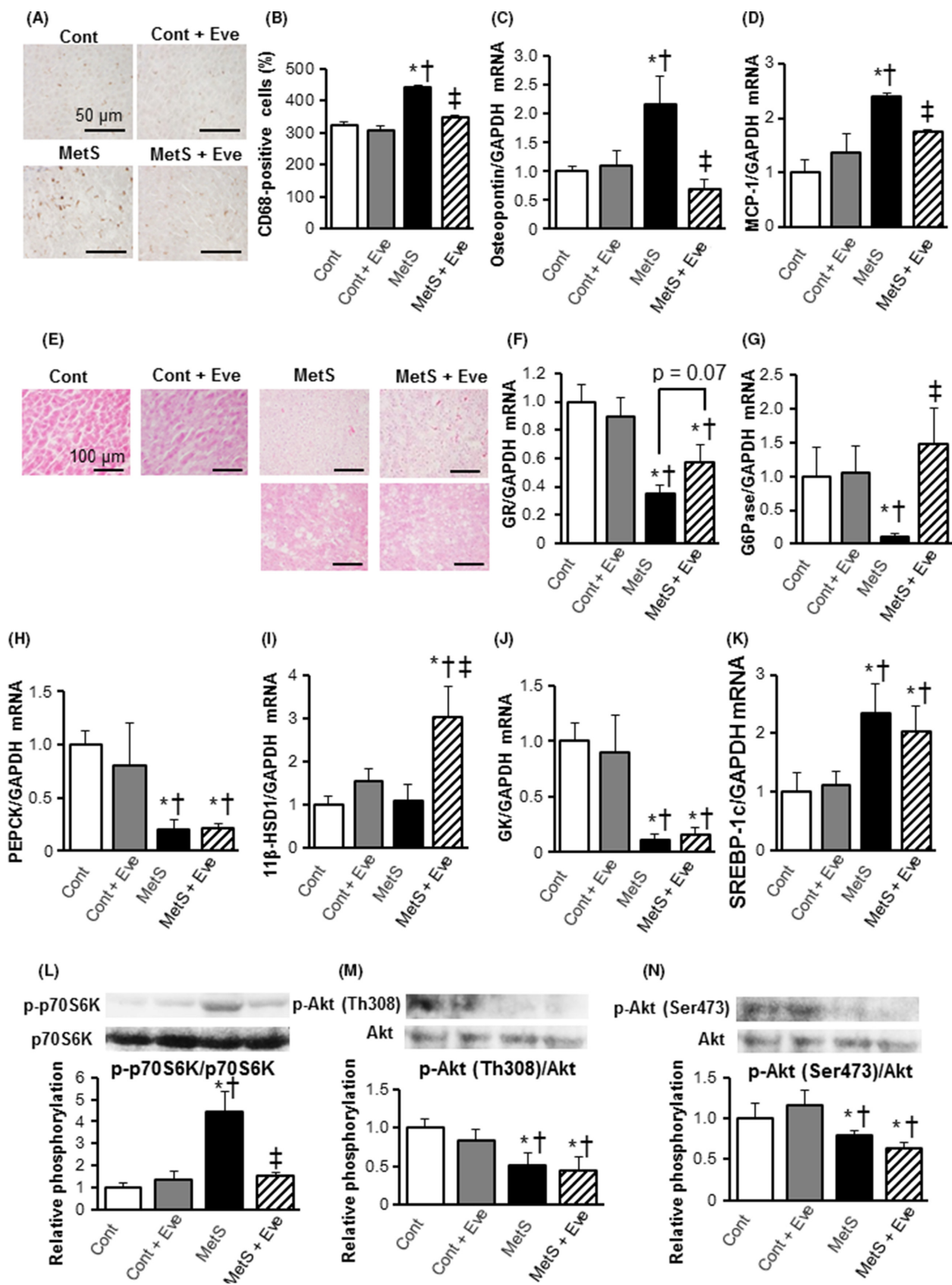
type 1(11β-HSD1) (Fig. 5I), were observed in the MetS group. Administration of everolimus significantly increased the expression level of G6Pase, and 11β-HSD1, and GR mRNA levels tended to increase in the MetS + Eve group when compared to that in the MetS group ($P = 0.07$). Meanwhile, the PEPCK gene level was not affected by everolimus (Fig. 5H). To further investigate the effect on glucose metabolism, we examined the glycolytic gene expression. Glucose uptake is mediated by glycolysis, and glucokinase (GK) is an essential enzyme in the regulation of rates of glycolysis. The expression level of GK was decreased in the MetS group, and everolimus did not influence its expression (Fig. 5J). Sterol regulatory element-binding protein 1c (SREBP-1c) is a key transcription factor that regulates the transcription of genes required for de novo lipogenesis. The expression level of SREBP-1c gene in the liver was enhanced in the MetS

group, and this increase was not affected by everolimus (Fig. 5K). Regarding insulin signal activities in the liver, phosphorylation levels of p70S6K and Akt, showed a pattern similar to that in the adipose tissue, the phosphorylation levels of Akt at Th308 or Ser473 were not influenced by administration of everolimus (Fig. 5L–N).

Glucose tolerance, insulin sensitivity, and pancreatic pathology

Glucose tolerance was impaired in the MetS group when compared with the Cont group and this impairment was exacerbated in the MetS + Eve group (Fig. 6A). In contrast, insulin sensitivity was decreased in the MetS group compared with that in the Cont group, and everolimus treatment had no effect on insulin sensitivity (Fig. 6B and
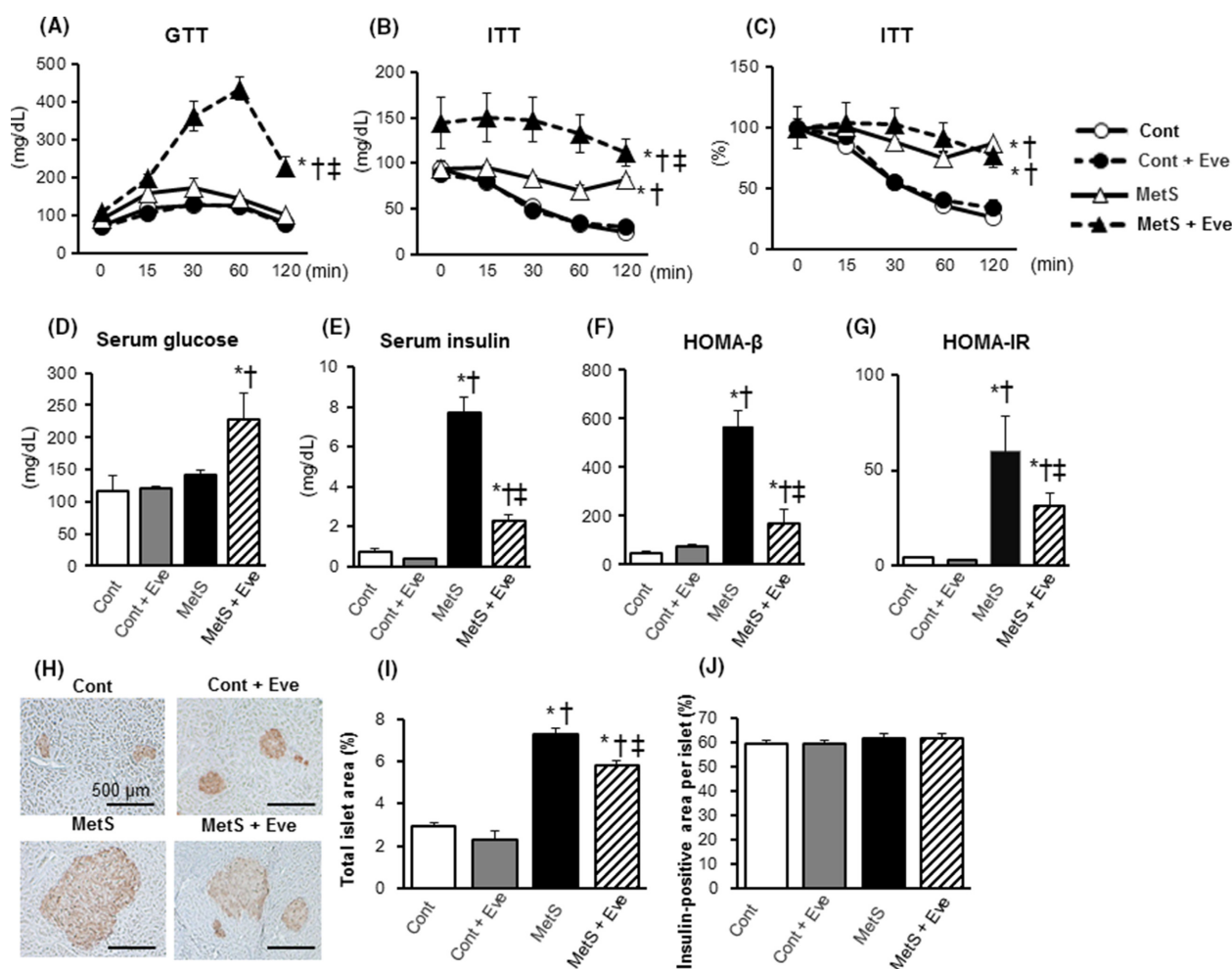

Figure 6. Glucose metabolism. (A–G) Effects on the oral glucose tolerance test (OGTT), the insulin tolerance test (ITT), the fasting serum glucose, the fasting serum insulin, HOMA-β, and HOMA-IR. (H) Immunohistochemistry of pancreatic sections stained for insulin and (I, J) its-associated morphological parameters. Scale bars, 500 μm. All quantitative data represent means ± SEM. [$n = 5, 6, 6$, and 7 (A–G) or $n = 8, 10, 7$, and 12 (I, J) for Cont, Cont + Eve, MetS, and MetS + Eve] *$P < 0.05$ versus Cont, †$P < 0.05$ versus Cont + Eve, ‡$P < 0.05$ versus MetS.

C). The fasting serum glucose levels in the MetS + Eve group was significantly higher than the Cont and Cont+Eve groups (Fig. 6D).The concentration of insulin in serum was increased in the MetS group, and this effect was markedly reduced in the MetS + Eve group (Fig. 6E). Both homeostasis model assessment (HOMA) for β-cell function (HOMA-β), an index of basal insulin secretion, and HOMA of insulin resistance (HOMA-IR), an index of insulin resistance, were increased in the MetS group compared to those in the Cont group and these effects were attenuated in the MetS + Eve group (Fig. 6F and G). Total islet area per field pancreatic area was greater in the MetS group than in the CONT group, and this effect was attenuated in the MetS + Eve group (Fig. 6H and I). Meanwhile, insulin positive area per islet cross-sectional area was not different in the four experimental groups (Fig. 6J).

Lipid metabolism

Serum levels of total cholesterol, low-density lipoprotein (LDL)-cholesterol, high-density lipoprotein (HDL)-cholesterol, triglyceride, and free fatty acid were significantly increased in the MetS group compared with the Cont group. These parameters did not differ between the MetS and MetS + Eve groups (Table S1).

Discussion

These data indicate that blockade of mTOR by everolimus attenuates obesity and hypertension as well as LV hypertrophy, fibrosis, and diastolic dysfunction in DS/obese rats. In addition, everolimus alleviated adipocyte hypertrophy and inflammatory responses in the visceral adipose and liver tissue of these rats. Meanwhile, everolimus exacerbated glucose intolerance in DS/obese rats. This effect was associated with a decrease in total islet area with no change in insulin-positive area per islet as well as increased expression of hepatic gluconeogenic genes. Figure S2 depicts a simplified representation of the inhibitory effects of everolimus on insulin signaling cascades in DS/obese rats.

The beneficial cardiac effects of everolimus were associated with the improvement of insulin signaling in the heart through reduction of mTOR/p70S6K-mediated negative feedback inhibition and with inhibition of cardiac oxidative stress and inflammation. Our previous study (Takatsu et al. 2013) showed that calorie restriction ameliorates hypertension, LV remodeling and diastolic dysfunction in DS/obese rats. In addition, suppression of mTOR during calorie restriction has been associated with amelioration of LV diastolic dysfunction associated with aging (Shinmura et al. 2011). Thus, in the present study,

the everolimus-induced reductions in food intake and body weight gain might be partially responsible for the prevention of hypertension and cardiac injury. However, these metabolic changes with everolimus in itself account for the beneficial effects on cardiac and adipose tissue pathology but not the detrimental effect on glucose metabolism. It is thus thought that the cardiac effects of everolimus are likely attributable to direct inhibition of mTOR in the heart as well as to antihypertensive and/or metabolic effects.

There are few reports on the role of mTOR in the regulation of blood pressure. In the vasculature, increased mTOR signaling has been observed in the aorta of mice fed a high-fat diet, which was associated with increased vascular senescence and dysfunction, and sensitivity to ischemic injury, which was reduced by rapamycin treatment (Wang et al. 2009). One previous study reported that rapamycin did not alter LV systolic or diastolic pressure in aortic-banded mice (Shioi et al. 2003). In our study, everolimus substantially attenuated hypertension in DS/obese rats. Given that treatment with everolimus diminished cardiac oxidative stress in DS/obese rats, the antihypertensive effect of everolimus in these animals may result from a reduced superoxide-dependent conversion of vasodilatory nitric oxide to peroxynitrite. Inflammation may generate an alteration of vascular function and thereby lead to hypertension. In DS/obese rats, everolimus inhibited cardiac inflammatory responses. Attenuation of hypertension by everolimus in DS/obese rats may thus be attributable, at least in part, to inhibition of vascular oxidative stress and inflammation. The reason for increased blood pressure induced by everolimus in DS/lean rats remains to be determined. However, unchanged LV mass in the presence of blood pressure elevation with everolimus in DS/lean rats suggests that attenuation of LV remodeling apparent in DS/obese rats might be at least partially independent of blood pressure.

An essential aspect in the preservation of glucose homeostasis is the maintenance of pancreatic β-cell mass and the ability of the β-cell mass to increase in response to insulin resistant states such as obesity (Jefferies et al. 1994). DS/obese rats exhibited increases in total islet area as well as no changes in insulin-positive area per islet, leading to an increase in β-cell mass. These findings are consistent with previous results demonstrating that hyperactivation of mTORC1 by energy-activated Rheb (Hamada et al. 2009) or inactivation of TSC1 (Mori et al. 2009) or TSC2 (Shigeyama et al. 2008), selectively in β-cells, led to increases in β-cell mass and proliferation. This expansion of β-cell mass is the result of increased generation of progenitor cells, hypertrophy, reduction in apoptosis, and increased enteric nutrient (especially fat) absorption. However, glucose tolerance was impaired in

DS/obese rats, suggesting that glucose-stimulated insulin secretion was reduced despite increased β-cell mass. Some reports suggest that rapamycin has critical effects on pancreatic β-cells. The combined evidence from studies investigating the direct effects of rapamycin on pancreatic β-cell function strongly suggests that rapamycin adversely affects glucose-stimulated insulin secretion from β-cells (Barlow et al. 2013). Although everolimus did not affect insulin-positive area per islet, it attenuated the increase in total islet area, leading to a loss in β-cell mass. Furthermore, elevated serum insulin level in DS/obese rats was markedly inhibited by everolimus administration. From these results, we speculate that everolimus negatively affected the insulin secretory property of pancreatic β-cells by blocking mTORC, leading to impaired glucose tolerance. However, the regulation of insulin secretion in β-cells involves many complex signaling pathways and, as such, the mechanisms by which mTOR may regulate insulin secretion remain unclear.

mTOR/p70S6K pathway is a critical signaling component in the development of obesity-related insulin resistance and regulates a negative feedback loop converging at PI3K/Akt pathway (Tuttle et al. 2001; Bhaskar and Hay 2007). mTORC1 blockage with everolimus downregulated the phosphorylation of p70S6K, but did not induce Akt activation despite a reduction in negative feedback inhibition in adipose and liver tissues. This may be because insulin signaling was impaired by the everolimus-induced decrease in insulin secretion from pancreatic β-cells.

Chronic everolimus treatment exacerbated glucose intolerance in DS/obese rats. Everolimus-induced deterioration of glucose intolerance is consistent with previous observations that chronic inhibition of mTORC by rapamycin causes hyperlipidemia, reduces fat mass, and promotes glucose intolerance as well as a diabetes-like syndrome (Houde et al. 2010; Lamming et al. 2012). A recent study reported that chronic administration of rapamycin leads to glucose intolerance and hyperlipidemia by elevating hepatic gluconeogenesis and impairing lipid deposition in the adipose tissue (Wang et al. 2015). The level of mRNA for PEPCK, a rate-limiting enzyme in gluconeogenesis, was decreased in the liver of DS/obese rats, and this effect was not affected by treatment with everolimus. However, the expression of mRNAs for G6Pase and 11β-HSD1, other gluconeogenic factors, was upregulated in the MetS + Eve group compared to that in the MetS group. The expression of the glycolysis gene, GK, is induced by insulin. Thus, in the MetS + Eve group, which showed reduction of insulin level, everolimus did not affect the expression of this gene despite inactivation of the mTOR/p70S6K-mediated negative feedback loop. Thus, chronic blockade of mTOR with everolimus activates gluconeogenesis, but not glycolysis, and this effect

also contributed to the deterioration of glucose metabolism. It is possible that the increase in water intake in the MetS+Eve group at 10 and 11 weeks is related to everolimus-induced hyperglycemia. However, despite the decrease in water intake after 12 weeks and thereafter, the MetS + Eve group displayed deterioration of glucose intolerance at 13 weeks. Future studies are needed to elucidate the mechanism for this effect of evelorimus.

Everolimus leads to activation of Akt via inhibition of mTORC1 negative feedback loop by binding to FK506-binding protein (FKBP12) (Schuler et al. 1997), while not inhibiting the mTORC2 positive feedback to Akt. mTORC2 phosphorylates Akt on Ser473 (Wang et al. 2015; Yang et al. 2015). A previous study demonstrated that hepatic mTORC2 inhibition results in decreased glucose uptake and enhanced gluconeogenesis by reduced Akt activity, especially loss of Akt Ser473 phosphorylation in the fed state (Hagiwara et al. 2012). Rapamycin directly inhibits mTORC1, and only chronic administration of rapamycin can inhibit mTORC2 (Sarbassov et al. 2006). Chronic rapamycin treatment aggravates glucose metabolism in diabetic subjects (Houde et al. 2010; Lamming et al. 2012). Chronic everolimus administration would have the same action as rapamycin for glucose metabolism via Akt Ser473 phosphorylation. However, the mechanism of inhibition of mTORC2 by everolimus remains to be fully elucidated. PI3K/Akt/mTORC/p70S6K signaling cascade and the mechanism of phosphorylation of Akt Ser473 are highly complex, and the activation of yet-to-be-defined pathways may exist. Thus, although we examined the effects of everolimus on Akt/mTORC/p70S6K signaling activities, the present results cannot fully explain this complex pathway.

On the other hand, everolimus exerted little influence on lipogenesis. Insulin activates the lipogenic gene, SREBP-1c, via Akt signaling (Li et al. 2010). Everolimus may have downregulated insulin secretion and the activation of its downstream signaling pathway. Therefore, everolimus had no effects on the expression level of SREBP-1c as well as serum levels of cholesterol and triglyceride.

Renal dysfunction, as shown by creatinine clearance, was significantly worsened by everolimus in DS/obese rats. This functional depression may have also been associated with impaired glucose metabolism. In contrast, urinary protein levels, the glomerulosclerosis index (GSI), and tubulointerstitial injury score (TIS) were not changed and renal inflammation was inhibited by administration of everolimus. Everolimus has been used as a growth inhibitor for kidney cancer and as an immunosuppressant for renal transplant in clinical practice (Sabbatini et al. 2015). Side effects such as a decline in renal function by this drug have not been reported (Takahashi et al. 2013; Sabbatini et al. 2015), and the present results are not consistent with these reports. Everolimus might not greatly

influence renal pathology, and our results suggest a need for further analyses.

At 9–13 weeks, all of the DS/obese rats are alive. DS/obese rats die after 15 week of age and their survival rate at 18 weeks was approximately 35% (Hattori et al. 2011). From 9 to 13 week, DS/obese rats present progressive hypertension, LV diastolic dysfunction, LV hypertrophy, fibrosis, and insulin resistance (Matsuura et al. 2015; Takeshita et al. 2015). Also, hyperphagia is gradually reduced after 11 weeks. Thus, we consider that this age range is suitable for evaluating the effects of this drug on MetS pathophysiology.

In conclusion, mTOR inhibition with everolimus ameliorated obesity as well as cardiac and adipose tissue pathology, but exacerbated glucose metabolism in DS/obese rats. Our results suggest that activation of mTOR signaling contributes to the pathophysiology of MetS and its associated complications.

Acknowledgement

Author Contribution

Participated in research design: Nagata. *Conducted experiments:* Uchinaka and Yoneda. *Performed data analysis:* Uchinaka, Yoneda, and Yamada. *Wrote or contributed to the writing of the manuscript:* Uchinaka, Murohara, and Nagata.

Disclosure

None declared.

References

Barlow AD, Nicholson ML, Herbert TP (2013). Evidence for rapamycin toxicity in pancreatic *β*-cells and a review of the underlying molecular mechanisms. Diabetes 62: 2674–2682.

Bhaskar PT, Hay N (2007). The two TORCs and Akt. Dev Cell 12: 487–502.

Buss SJ, Muenz S, Riffel JH, Malekar P, Hagenmueller M, Weiss CS, et al. (2009). Beneficial effects of mammalian target of rapamycin inhibition on left ventricular remodeling after myocardial infarction. J Am Coll Cardiol 54: 2435–2446.

Elmarakby AA, Loomis ED, Pollock JS, Pollock DM (2005). NADPH oxidase inhibition attenuates oxidative stress but not hypertension produced by chronic ET-1. Hypertension 45: 283–287.

Goudar RK, Shi Q, Hjelmeland MD, Keir ST, McLendon RE, Wikstrand CJ, et al. (2005). Combination therapy of inhibitors of epididymis growth factor receptor/vascular endothelial growth factor receptor 2 (AEE788) and the mammalian target of rapamycin (RAD001) offers improved glioblastoma tumor growth inhibition. Mol Cancer Ther 4: 101–112.

Hagiwara A, Cornu M, Cybulski N, Polak P, Betz C, Trapani F, et al. (2012). Hepatic mTORC2 activates glycolysis and lipogenesis through Akt, glucokinase, and SREBP1c. Cell Metab 15: 725–738.

Hamada S, Hara K, Hamada T, Yasuda H, Moriyama H, Nakayama R, et al. (2009). Upregulation of the mammalian target of rapamycin complex 1 pathway by Ras homolog enriched in brain in pancreatic *β*-cells leads to increased *β*-cell mass and prevention of hyperglycemia. Diabetes 58: 1321–1332.

Hattori T, Murase T, Ohtake M, Inoue T, Tsukamoto H, Takatsu M, et al. (2011). Characterization of a new animal model of metabolic syndrome: the DahlS.Z-Leprfa/Leprfarat. Nutr. Diabetes 1: e1.

Hausleiter J, Kastrati A, Mehilli J, Vogeser M, Zohlnhöfer D, Schühlen H, et al. (2004). Randomized, double-blind, placebo-controlled trial of oral sirolimus for restenosis prevention in patients with in-stent restenosis: the oral sirolimus to inhibit recurrent in-stent stenosis (OSIRIS) trial. Circulation 110: 790–795.

Houde VP, Brûlé S, Festuccia WT, Blanchard PG, Bellmann K, Deshaies Y, et al. (2010). Chronic rapamycin treatment causes glucose intolerance and hyperlipidemia by upregulating hepatic gluconeogenesis and impairing lipid deposition in adipose tissue. Diabetes 59: 1338–1348.

Hughes KJ, Kennedy BK (2012). Cell biology. Rapamycin paradox resolved. Science 335: 1578–1579.

Jefferies HB, Reinhard C, Kozma SC, Thomas G (1994). Rapamycin selectively represses translation of the "polypyrimidine tract" mRNA family. Proc Natl Acad Sci USA 91: 4441–4445.

Kato MF, Shibata R, Obata K, Miyachi M, Yazawa H, Tsuboi K, et al. (2008). Pioglitazone attenuates cardiac hypertrophy in rats with salt-sensitive hypertension: role of activation of AMP-activated protein kinase and inhibition of Akt. J Hypertens 26: 1669–1676.

Lamming DW, Ye L, Katajisto P, Goncalves MD, Saitoh M, Stevens DM, et al. (2012). Rapamycin-induced insulin resistance is mediated by mTORC2 loss and uncoupled from longevity. Science 335: 1638–1643.

Laplante M, Sabatini DM (2012). mTOR signaling in growth control and disease. Cell 149: 274–293.

Li S, Brown MS, Goldstein JL (2010). Bifurcation of insulin signaling pathway in rat liver: mTORC1 required for stimulation of lipogenesis, but not inhibition of gluconeogenesis. Proc Natl Acad Sci USA 107: 3441–3446.

Mancini M, Petta S, Martinelli G, Barbieri E, Santucci MA (2010). Rad 001 (everolimus) prevents mTOR and Akt late reactivation in response to imatinib in chronic myeloid leukemia. J Cell Biochem 109: 320–328.

Matsuura N, Asano C, Nagasawa K, Ito S, Sano Y, Minagawa Y, et al. (2015). Effects of pioglitazone on cardiac and adipose tissue pathology in rats with metabolic syndrome. Int J Cardiol 179: 360–369.

Mori H, Inoki K, Opland D, Münzberg H, Villanueva EC, Faouzi M, et al. (2009). Critical roles for the TSC-mTOR pathway in β-cell function. Am J Physiol Endocrinol Metab 297: E1013–E1022.

Murase T, Hattori T, Ohtake M, Abe M, Amakusa Y, Takatsu M, et al. (2012a). Cardiac remodeling and diastolic dysfunction in DahlS.Z-Leprfa/Leprfarats: a new animal model of metabolic syndrome. Hypertens Res 35: 186–193.

Nagata K, Somura F, Obata K, Odashima M, Izawa H, Ichihara S, et al. (2002). AT1 receptor blockade reduces cardiac calcineurin activity in hypertensive rats. Hypertension 40: 168–174.

Nagata K, Obata K, Xu J, Ichihara S, Noda A, Kimata H, et al. (2006). Mineralocorticoid receptor antagonism attenuates cardiac hypertrophy and failure in low-aldosterone hypertensive rats. Hypertension 47: 656–664.

Sabbatini M, Ruggiero G, Palatucci AT, Rubino V, Federico S, Giovazzino A, et al. (2015). Oscillatory mTOR inhibition and Treg increase in kidney transplantation. Clin Exp Immunol 182: 230–240.

Sarbassov DD, Ali SM, Sengupta S, Sheen JH, Hsu PP, Bagley AF, et al. (2006). Prolonged rapamycin treatment inhibits mTORC2 assembly and Akt/PKB. Mol Cell 22: 159–168.

Schuler W, Sedrani R, Cottens S, Háberlin B, Schulz M, Schuurman HJ, et al. (1997). SDZ RAD, a new rapamycin derivative: pharmacological properties in vitro and in vivo. Transplantation 64: 36–42.

Shigeyama Y, Kobayashi T, Kido Y, Hashimoto N, Asahara S, Matsuda T, et al. (2008). Biphasic response of pancreatic β-cell mass to ablation of tuberous sclerosis complex 2 in mice. Mol Cell Biol 28: 2971–2979.

Shinmura K, Tamaki K, Sano M, Murata M, Yamakawa H, Ishida H, et al. (2011). Impact of long-term caloric restriction on cardiac senescence: caloric restriction ameliorates cardiac diastolic dysfunction associated with aging. J Mol Cell Cardiol 50: 117–127.

Shioi T, McMullen JR, Tarnavski O, Converso K, Sherwood MC, Manning WJ, et al. (2003). Rapamycin attenuates load-induced cardiac hypertrophy in mice. Circulation 107: 1664–1670.

Stone GW, Sabik JF, Serruys PW, Simonton CA, Généreux P, Puskas J, et al. (2016). Everolimus-eluting stents or bypass surgery for left main coronary artery disease. N Engl J Med 375: 2223–2235.

Takahashi K, Uchida K, Yoshimura N, Takahara S, Teraoka S, Teshima R, et al. (2013). Efficacy and safety of concentration-controlled everolimus with reduced-dose cyclosporine in Japanese de novo renal transplant patients: 12-month results. Transplant Res 2: 14.

Takatsu M, Nakashima C, Takahashi K, Murase T, Hattori T, Ito H, et al. (2013). Calorie restriction attenuates cardiac remodeling and diastolic dysfunction in a rat model of metabolic syndrome. Hypertension 62: 957–965.

Takeshita Y, Watanabe S, Hattori T, Nagawsawa K, Matsuura N, Takahashi K, et al. (2015). Blockade of glucocorticoid receptors with RU486 attenuates cardiac damage and adipose tissue inflammation in a rat model of metabolic syndrome. Hypertens Res 38: 741–750.

Tuttle RL, Gill NS, Pugh W, Lee JP, Koeberlein B, Furth EE, et al. (2001). Regulation of pancreatic β-cell growth and survival by the serine/threonine protein kinase Akt1/PKBα. Nat Med 7: 1133–1137.

Wang CY, Kim HH, Hiroi Y, Sawada N, Salomone S, Benjamin LE, et al. (2009). Obesity increases vascular senescence and susceptibility to ischemic injury through chronic activation of Akt and mTOR. Sci Signal 2: ra11.

Wang Y, He Z, Li X, Chen W, Lu J, Chen X, et al. (2015). Chronic rapamycin treatment exacerbates metabolism and does not down-regulate mTORC2/Akt signaling in diabetic mice induced by high-fat diet and streptozotocin. Pharmazie 70: 604–609.

Yang G, Murashige DS, Humphrey SJ, James DE (2015). A Positive Feedback Loop between Akt and mTORC2 via SIN1 Phosphorylation. Cell Rep 12: 937–943.

Yuan R, Kay A, Berg WJ, Lebwohl D (2009). Targeting tumorigenesis: development and use of mTOR inhibitors in cancer therapy. J Hematol Oncol 2: 45.

Supporting Information

Additional Supporting Information may be found online in the supporting information tab for this article:

Data S1. Materials and Methods.
Table S1. Metabolic parameters of DS/lean and DS/obese rats in the four experimental groups at 13 weeks of age.
Figure S1. Renal histological changes induced by everolimus in DS/obese rats.
Figure S2. Schematic representation of mammalian target of rapamycin (mTOR) inhibitor everolimsin on glucose metabolism and insulin signal in rat with metabolic symdorome via mTOR/p70S6K/Akt pathway and insulin secretion from pancreatic β-cells.